A NOVEL APPROACH OF INITIALIZING REGION-BASED ACTIVE CONTOURS IN NOISY IMAGES BY MEANS OF UNIMODALITY ANALYSIS

Kevin Ohliger[1], *Torsten Edeler*[1], *Alexandru P. Condurache*[2], *Alfred Mertins*[2]

[1]: Institute for Machine Vision Technology, Westcoast University of Applied Sciences, 25746 Heide, Germany
[2]: Institute for Signal Processing, University of Lübeck, 23538 Lübeck, Germany
Email: ohliger@fh-westkueste.de

ABSTRACT

In this paper a novel approach of initializing region-based active contours using unimodality analysis is introduced. Two different initialization methods using dip test and excess mass test to adapt the initial radii of the active contours are developed. Both methods are compared to state of the art methods and a method which is based on kurtosis and dissimilarity (KDR). It is shown that the excess mass method outperforms KDR and state of the art methods for synthetic and real images for different noise setups with respect to the overall accuracy and Cohen's kappa of the segmentation results.

***Index Terms*—active contours, initialization, dip test, unimodality, multimodality, excess mass, overall accuracy, Cohen's kappa, KDR, segmentation**

I. INTRODUCTION

Segmentation of a scene is still a challenging task and thus a topic of current research. In 1988 Kass et al. introduced in [1] a new segmentation method based on active contour models, also called snakes, using local edge information. This segmentation method was successfully applied for different applications in [2], [3]. The problems caused by the edge detectors are their sensitivity to noise and discontinuous boundaries in the image as shown in [4]. They were first substituted by region-based approaches in [5]. Related to the Mumford-Shah functional Chan and Vese [4] developed an active contour model assuming that an image is piecewise constant and Osher and Sethian [6] introduced level sets that allow topological changes of the contours.

In [7], [8], [9], [10] geodesic active contour algorithms were developed, for which the initialization step is not crucial. Bresson et al. [11] introduced a fast global minimization of the active contour model which is based on the combination of segmentation and denoising without depending on initial contour positions. Nevertheless most active contour algorithms need an appropriate initialization of the starting contours. These contours have significant influence on the segmentation result as it is shown in [12]. The different initializations may lead to local minima of the functional energy of the active contours and not to the desired global minimum.

There exist only a few initialization methods in literature up to now. The easiest and probably best initialization is done manually by the user as described in [13], [14], [15]. Another common method for initializing the active contours are seed contours placed in a regular grid in the image [13], [16], [17] while no adaptation of the grid pitch or initial contour size to image data are made. We showed in [12] that an adaptation of the initial radii of the active contours lead to more accurate segmentation results. The proposed methods initialize the contours by using two different unimodality measures. This approach is related to the initialization method introduced by Ohliger et al. in [12].

The outline of the paper is as follows. After introducing our active contour model in Section II and our image model in Section III we derive two novel methods for adaptation of the initial contours. In Section V experimental results on synthetic and real images are discussed and finally we conclude in Section VI.

II. ACTIVE CONTOUR MODEL

The energy of a classical active contour (AC) model E_{AC} (see [1]) consists of an internal energy E_{int} and an external energy E_{ext}

$$E_{\mathrm{AC}}(u, C) = E_{int}(C) + E_{ext}(u, C). \tag{1}$$

E_{int} depends on the contour C only and forces the contour to become smooth and E_{ext} includes the influence of the function u describing the image. We use a region-based AC model introduced by [5] defining the energy of a single contour i

$$E_{\mathrm{AC},i}(u, C_i, \theta_{\mathbf{i}}) = \frac{\mu}{2}\mathrm{Length}(C_i) - \iint\limits_{(x,y)\in R_i} \ln P(u(x,y) \mid \theta_{\mathbf{i}})\, dx\, dy. \tag{2}$$

R_i is the region enclosed by contour C_i and $\theta_{\mathbf{i}}$ contains the statistical parameters describing a feature probability density function of R_i. $\mathrm{Length}(C_i)$ is the length of the boundary curve and μ a positive weighting factor for the smoothness term. The segmentation is achieved by minimizing the energy of the contour set C including P contours C_i

$$\begin{aligned}\tilde{\mathbf{C}} &= \arg\min_{C_i\in C} \sum_{i=1}^{P}\left[E_{\mathrm{AC}}(u, C_i, \theta_{\mathbf{i}}) + \lambda\right] \\ &= \arg\min_{C_i\in C} \sum_{i=1}^{P}\left[\frac{\mu}{2}\mathrm{Length}(C_i) - \iint\limits_{(x,y)\in R_i} \ln P(u(x,y) \mid \theta_{\mathbf{i}})\, dx\, dy + \lambda\right].\end{aligned} \tag{3}$$

λ is a positive constant for avoiding oversegmentation and $\tilde{\mathbf{C}}$ is the set of final contours.

The parameters $\theta_{\mathbf{i}}$ are estimated based on the sampled image data matrix $\mathbf{U_0}$ with dimension K x L. We assume that $\mathbf{U_0}$ contains M different objects ω_j with features (e.g. intensity values) that can be described by unimodal Gaussian distributions $\mathcal{N}\left(\mu_{\omega_j}, \sigma^2_{\omega_j}\right)$.

978-1-4244-5899-8/10/$26.00 ©2010 IEEE

μ_{ω_j} and $\sigma^2_{\omega_j}$ are the feature means and variances of the respective object. The parameters

$$\theta_i = [\theta_{i0}, \theta_{i1}] = [\mu_{R_i}, \sigma^2_{R_i}] \tag{4}$$

of a unimodal Gaussian distribution $\mathcal{N}(\theta_{i0}, \theta_{i1})$ for Region R_i are estimated by

$$\theta_{i0} = \sum_{j=1}^{M} \alpha_{ji} \cdot \mu_{\omega_j} \tag{5}$$

and

$$\theta_{i1} \approx \frac{N_{R_i}}{N_{R_i} - 1} \sum_{j=1}^{M} \alpha_{ji} \left[\sigma^2_{\omega_j} + \left(\mu_{R_i} - \mu_{\omega_j} \right)^2 \right], \tag{6}$$

while α_{ji} describes the ratio of ω_j outcomes in region R_i to complete count of outcomes N_{R_i} of R_i. Due to the approximation of a χ^2 distribution included by the derivation of (6) the approximation of the variance leads to good results for N_{R_i} >100.

III. IMAGE MODEL

In this section we introduce the image model used. As mentioned in Section II the undistorted image data $\mathbf{U_0}$ is assumed to include $M \in [2, K \cdot L]$ different objects

$$u_0(k,l) = \sum_{j=1}^{M} f_{\omega_j}(k,l), \tag{7}$$

with $k = 1, \ldots, K$, $l = 1, \ldots, L$, and

$$f_{\omega_j}(k,l) = \begin{cases} F_j(k,l) & k,l \text{ inside of } \omega_j \\ 0 & \text{otherwise.} \end{cases} \tag{8}$$

$\mathbf{F}_j$ is described by

$$\mathbf{F}_j \sim \mathcal{N}\left(\mu_{\omega_j}, \sigma^2_{\omega_j}\right). \tag{9}$$

We extend our model (7) with additive noise $\mathbf{N}$ resulting in the noisy image

$$\mathbf{U} = \mathbf{U_0} + \mathbf{N}, \tag{10}$$

while $\mathbf{N}$ is independent identically distributed noise. We concentrate on additive white Gaussian noise with zero mean and variance σ_n^2

$$\mathbf{N_g} \sim \mathcal{N}\left(0, \sigma_n^2\right). \tag{11}$$

IV. INITIALIZING THE CONTOURS

Our approach for selection of the initial contours (ICs) is based on the analysis of the probability density function (pdf) of the respective feature. According to our image model (10) the pdf inside a contours C_i, which contains one single object, is expected to be a unimodal Gaussian distribution distorted by noise. If a region R_i includes more than one object the pdf is assumed to have two or more modes. This assumption is valid if

$$\forall_{\omega_j, \omega_k \in R_i} \; \exists \, \mu_j \neq \mu_k. \tag{12}$$

Our image model also includes noise. This will lead to degraded pdfs dependent on the energy and type of the noise. The following sections introduce different statistical methods for testing of multimodality. The initialization of the contours is done by decreasing the starting initial contour with radius $r_0 = d_0/2$ placed on a regular grid with spatial pitch d_0 until the multimodality measure of the respective method is less than a threshold. We investigate in Section IV-A and Section IV-B the behavior of two multimodality measures with respect to multimodality and noise influence. The experiments were made on a sample set including 100 samples and a mixture of $\mathcal{N}_1(0.25, 0.01)$ and $\mathcal{N}_2(0.75, 0.01)$ while $\alpha_1 = 1 - \alpha_2$ describes the relative sample count of $\mathcal{N}_1$. All experiments were repeated 100 times.

IV-A. Hartigan's Dip Test Method (DT)

Hartigan and Hartigan introduced in [18] the dip test of unimodality. The dip is defined as

$$D(F) = \rho(F, \mathfrak{U}), \tag{13}$$

while

$$\rho(F, G) = \sup_x |F(x) - G(x)|. \tag{14}$$

F, G are bounded distribution functions and $\mathfrak{U}$ is the class of unimodal distribution functions. (13) leads to $D(F) = 0$ for $F \in \mathfrak{U}$ and to $D(F) > 0$ otherwise.

Multimodality: As shown in Fig. 1 the dip test for unimodality leads to rejection rates greater than 85% if at least 30% of the sample set are outcomes of the minor distribution ($\alpha_2 \geq 0.3$). The variance of the rejection rate decreases with α_2.

Noise Dependency: The noise dependency of the dip test for unimodality is shown in Fig. 2. The rejection rate is strongly influenced by the additive Gaussian noise. The mean rejection rate of an equal mixture ($\alpha_1 = \alpha_2$) decreases from approximately 1.0 to 0.3 by adding Gaussian noise with variance 4e-2 to the sample set. This results in a need for a noise adaptive threshold for the dip test.

IV-B. Excess Mass Method (EM)

In [19] Müller and Sawatzki introduced a new test for multimodality called excess mass test. The excess mass for a specified level λ is defined as

$$E(\lambda) = \int \left(\hat{f}(x) - \lambda \right)^+ dx \tag{15}$$

representing the integrated probability mass exceeding the Lebesgue density λ. For determining the excess mass of a unimodal distribution, $\hat{f}(x)$ is estimated by $\mathcal{N}\left(\mu, \sigma^2\right)$ while μ and σ^2 are the empirical mean and variance estimations.

$$E_M(\lambda) = \sup \sum_{i=1}^{M} \int_{C_i(\lambda)} \left(\hat{f}_j(x) - \lambda \right)^+ dx, \tag{16}$$

is the excess mass of a multimodal distribution containing M modes. $C_i(\lambda)$ is a cluster of connectivity components at level λ and $\hat{f}_j(x)$ is the estimated unimodal distribution based on the samples included in $C_i(\lambda)$. The excess mass test between a unimodal distribution and an M-modal distribution includes the maximal excess mass difference

$$\sup_\lambda D_M(\lambda) = \sup_\lambda \left(E_M(\lambda) - E_1(\lambda) \right). \tag{17}$$

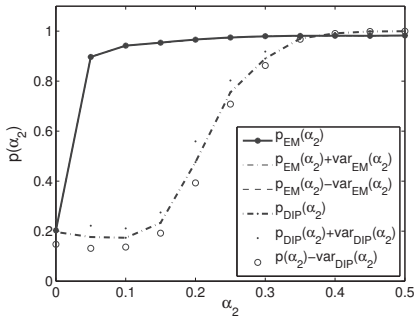

Fig. 1. Empirically determined p-value using critical bandwidth estimates for bimodal distributions depending on α_2.

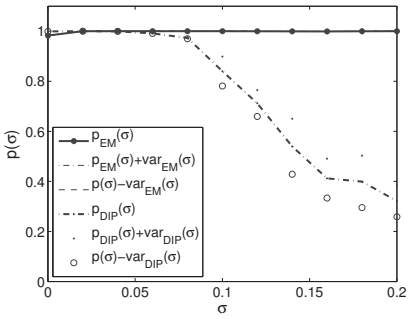

Fig. 2. Empirically determined p-value using critical bandwidth estimates for bimodal distributions depending on the noise variance σ^2.

The excess mass test for multimodality succeeds if (17) exceeds a specified threshold value. In our investigations we use the excess mass test between a unimodal and bimodal distribution.

Multimodality: As shown in Fig. 1 the excess mass test lead to high rejection rates $p(\alpha_2) \geq 0.9$ for $\alpha_2 \geq 0.05$. The variance of the rejection rate is in our setup negligible. This behavior of the rejection is expected to be a much better multimodality measure than the dip test.

Noise Dependency: The noise dependency of the EM is, as shown in Fig. 2, insignificant within the considered noise range. Also the variance of the test is very low. Both characteristics are expected to give a good measure for multimodality also for noisy sample sets.

V. EXPERIMENTAL RESULTS

To evaluate the methods for contour initialization, the segmentation results for a synthetic image fulfilling our image model (10) and for two real images are compared. We use the overall accuracy (OA) and Cohen's kappa (κ) [20] as measures for the accuracy of segmentation. The centers of the ICs are placed on a regular grid with pitch d_0, the initial radius is $0.5 \cdot d_0$ the minimum radius is r_{min}.The parameter of the AC energy (4) including λ and μ are fixed for each configuration of the input image in order to provide comparability of the segmentation results. Between the different images and different noise levels the parameters are configured to provide accurate results. The experimental results are focussing on the ICs selection and not on the optimal parameter for energy minimization of the AC.

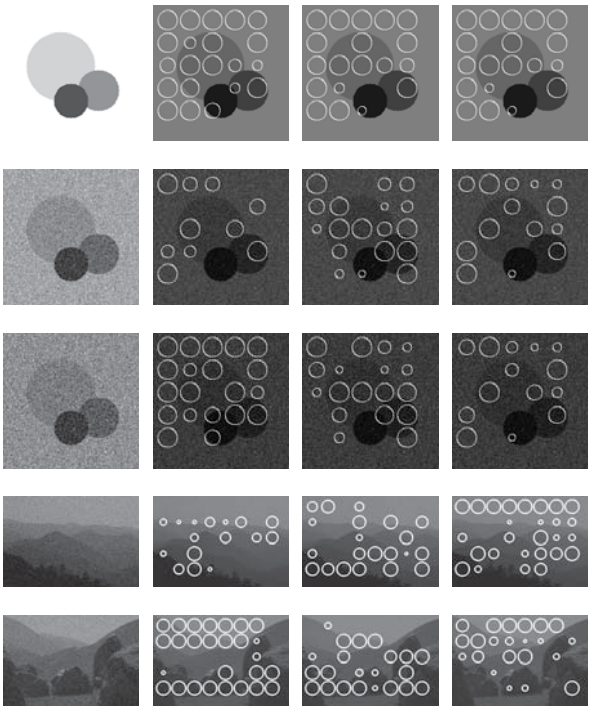

Fig. 3. Row 1-3 (a): Synthetic image with noise σ_n^2 = 1e-8 (1), σ_n^2 = 4e-2 (2), σ_n^2 = 9e-2 (3); Row 4-5 (a): Real images with σ_n^2 = 4e-2; Column (b)-(d) ICs of KDR (b), DT (c), and EM (d). Column (a) is scaled to [0,1] and (b)-(d) are scaled to [0,0.8] excluding the contours. Row 1-3: $d_0 = 30$ and $r_{\min} = 5$;Row 4-5: $d_0 = 50$ and $r_{\min} = 5$.

V-A. Synthetic Image

The synthetic image generated for evaluation of the different methods contains three overlapping circular objects ω_1, ω_2, ω_3, and a background ω_{bg} with the respective means $\mu_{bg} = 1$, $\mu_1 = 0.2$, $\mu_2 = 0.5$, and $\mu_3 = 0.8$.

Fig. 3 shows the initialization of KDR, DT and EM methods. Row 1 shows that even in an image with little noise the KDR method leads to contours containing more than one object (e.g. ω_1 and ω_{bg}) while DT and EM lead to accurate ICs. In row 2 and 3 KDR and DT lead to several inaccurate contours. The excess mass method leads in all noise conditions to the best ICs with the drawback of a lower contour count than for KDR and DT. The accuracies of the segmentation results are listed in Table I. The first row of Table I includes the best segmentation results for a fixed $r_0 \in \{5, 10, 15\}$. The segmentation resulting from EM initialization performs best excluding κ at noise variance $\sigma_n^2 = 4e{-}2$ where it is similar to the best result (fixed $r_0 = 5$). The KDR lead to similar results for low noise setups while DT segmentation was worst.

TABLE I
SEGMENTATION ACCURACY FOR SYNTHETIC AND REAL IMAGES WITH ADDITIVE GAUSSIAN NOISE

	Synth.		Synth.		Synth.		Real 1		Real 2	
	1e-8		4e-2		9e-2		4e-2		4e-2	
	OA	κ	OA	κ	OA	κ	OA	κ	OA	κ
Fix	**1.0**	**1.0**	**0.99**	**0.95**	0.96	0.83	0.89	0.87	0.79	0.76
KDR	**1.0**	**1.0**	0.98	0.93	0.97	0.88	0.90	0.88	0.78	0.75
DT	**1.0**	**1.0**	0.97	0.89	0.95	0.81	0.90	0.88	0.76	0.72
EM	**1.0**	**1.0**	**0.99**	0.94	**0.98**	**0.90**	**0.91**	**0.89**	**0.80**	**0.77**

V-B. Real Images

The evaluation of the segmentation results for real images was made on two different images of the Berkeley segmentation dataset[1] which were scaled to $[0, 1]$ and distorted by additive Gaussian noise with variance σ_n^2 = 4e-2. We expect the images to be compatible to our image model. The segmentation reference was also available in the dataset.
In Fig. 3 (row 4 and 5) the ICs for the different initialization methods are shown. Although the skies in both images are expected to be unimodal rows 4 and 5 in Fig. 3 show that KDR and DT reject many of ICs in this part. The EM method leads to a much better initialization of the ACs. The accuracies of the segmentation results are listed in Table I. The first row includes the best segmentation results for a fixed $r_0 \in \{5, 10, 15, 20, 25\}$. EM leads to best results also for real images while the performances of KDR and DT are similar.

VI. CONCLUSIONS

In this paper we introduced the DT and EM methods based on the novel approach of initializing active contours utilizing unimodality analysis. Both adapt the radii of the initial contours driven by image data. They were evaluated against state of the art initialization methods and the KDR method on synthetic and real images containing additive Gaussian noise. The EM method outperforms all other methods while the DT method leads to similar results as the KDR method.

VII. ACKNOWLEDGEMENT

This work is part of a project which is supported by the European Union (EFRE) and the federal state of Schleswig-Holstein, Germany (Zukunftsprogramm Wirtschaft).

VIII. REFERENCES

[1] M. Kass, A. Witkins, and D. Terzopoulus, "Snakes: active contour models," *International Journal of Computer Vision*, vol. 1, no. 4, 1988.

[2] L. Cohen, "On active contour models and balloons," *CVGIP. Image understanding*, vol. 53, no. 2, pp. 211–218, 1991.

[3] R. Malladi and J. Sethian, "A real-time algorithm for medical shape recovery," *IEEE Trans. Pattern Anal. Mach. Intell.*, vol. 14, no. 1, pp. 158–175, 1995.

[4] T. Chan and L. Vese, "Active contours without edges," *IEEE Trans. Image Process.*, vol. 10, no. 2, pp. 266–277, 2001.

[5] S. Zhu and A. Yuille, "Region competition: unifying snakes, region growing, and bayes/mdl for multiband image segmentation," *IEEE Trans. Pattern Anal. Mach. Intell.*, vol. 18, no. 9, pp. 884–900, 1996.

[6] S. Osher and J. Sethian, "Fronts propagating with curvature-dependent speed: algorithms based on hamilton-jacobi formulations," *Journal of computational physics*, vol. 79, no. 1, pp. 12–49, 1988.

[7] V. Caselles, R. Kimmel, and G. Sapiro, "Geodesic active contours." IEEE Comput. Soc. Press, 1995, pp. 694–699.

[8] S. Kichenassamy, A. Kumar, P. Olver, A. Tannenbaum, and A. Yezzi, "Gradient flows and geometric active contour models." IEEE Comput. Soc. Press, 1995, pp. 810–815.

[9] R. Malladi, J. Sethian, and B. Vemuri, "Shape modeling with front propagation: a level set approach," *IEEE Transactions on Pattern Analysis and Machine Intelligence*, vol. 17, no. 2, pp. 158–175, 1995.

[10] N. Paragios and R. Deriche, "Geodesic active regions for supervised texture segmentation," in *Computer Vision, 1999. The Proceedings of the Seventh IEEE International Conference on*, vol. 2, 1999, pp. 926 –932 vol.2.

[11] X. Bresson, S. Esedoglu, P. Vandergheynst, J.-P. Thiran, and S. Osher, "Fast global minimization of the active contour/snake model," *Journal of Mathematical Imaging and Vision*, vol. 28, no. 2, pp. 151–167, Aug 2007.

[12] K. Ohliger, T. Edeler, S. Hussmann, A. P. Condurache, and A. Mertins, "A novel approach of initializing region-based active contours in noisy images by means of higher order statistics and dissimilarity," in *International Conference on Mechatronics and Automation*, 2010, to appear.

[13] T. McInerney and D. Terzopoulus, "Topologically adaptable snakes," in *IEEE Fifth Int. Conf. on Computer Vision*, 1995.

[14] A. Tsai, A. Yezzi, and A. Willsky, "Curve evolution implementation of the mumford-shah functional for image segmentation, denoising, inerpolation and magnification," *IEEE Trans. Image Process.*, vol. 10, no. 8, pp. 1169–1186, 2001.

[15] H. Li and L. Cohen, "3d brain segmentation using dual-front active contours with optional user interaction," *International Journal of Biomedical Imaging*, vol. 2006, pp. 1–17, 2006.

[16] J. A. Yezzi, A. Tsai, and A. Willsky, "A statistical approach to snakes for bimodal and trimodal imagery," in *The Proceedings of the Seventh IEEE International Conference on Computer Vision, 1999*, vol. 2, 1999.

[17] P. Martin, P. Refregier, F. Goudail, and F. Guerault, "Influence of the noise model on level set active contour segmentation," *IEEE Transactions on Pattern Analysis and Machine Intelligence*, vol. 26, no. 6, pp. 799–803, Jun 2004.

[18] J. Hartigan and P. Hartigan, "The dip test of unimodality," *The Annals of Statistics*, vol. 13, no. 1, pp. 70–84, 1985.

[19] D. W. Muller and G. Sawitzki, "Excess mass estimates and tests for multimodality," *Journal of the American Statistical Association*, vol. 86, no. 415, p. 738, Sep 1991.

[20] J. Cohen *et al.*, "A coefficient of agreement for nominal scales," *Educational and psychological measurement*, vol. 20, no. 1, pp. 37–46, 1960.

[1] http://www.eecs.berkeley.edu/Research/Projects/CS/vision/bsds/